LAWRENCE
LIVERMORE
NATIONAL
LABORATORY

LLNL-JRNL-646742

First measurements of hydrodynamic instability growth in indirectly driven implosions at the National Ignition Facility

V. A. Smalyuk, D. T. Casey, D. S. Clark, M. J. Edwards, S. W. Haan, A. Hamza, D. E. Hoover, W. W. Hsing, O. Hurricane, J. D. Kilkenny, J. Kroll, O. L. Landen, A. Moore, A. Nikroo, L. Peterson, K. Raman, B. A. Remington, H. F. Robey, S. V. Weber, K. Widmann

November 22, 2013

Physical Review Letters

Disclaimer

First measurements of hydrodynamic instability growth in indirectly driven implosions at the National Ignition Facility

V. A. Smalyuk[1], D. T. Casey[1], D. S. Clark[1], M. J. Edwards[1], S. W. Haan[1], A. Hamza[1], D. E. Hoover[2], W. W. Hsing[1], O. Hurricane[1], J. D. Kilkenny[2], J. Kroll[1], O. L. Landen[1], A. Moore[3], A. Nikroo[2], L. Peterson[1], K. Raman[1], B. A. Remington[1], H. F. Robey[1], S. V. Weber[1], and K. Widmann[1]

[1]Lawrence Livermore National Laboratory, Livermore, CA 94550

[2]General Atomics, San Diego, CA 92121

[3]AWE Aldermaston, Reading, Berkshire, RG7 4PR, United Kingdom.

ABSTRACT

The first hydrodynamic instability growth measurements in indirectly driven implosions on the National Ignition Facility are presented. Plastic capsules had two-dimensional pre-imposed, sinusoidal modulations at the outer capsule surface with initial wavelengths of 240 μm (corresponding to Legendre mode number of 30), 120 μm (mode 60), and 80 μm (mode 90). The capsules were imploded using ignition-relevant laser pulses, and ablation-front modulation growth was measured using x-ray radiography for shell distance travelled up to 600 μm. The measured growth was in good agreement with that predicted for all three modes, validating simulations for the fastest growing modulations with mode numbers up to 90 in the acceleration phase. Future experiments will be focused on measurements at higher convergence, higher-mode number modulations, and occurring during the deceleration phase.

Hydrodynamic instabilities and mix play a central role in the performance degradation of the spherical implosions in inertial confinement fusion (ICF) [1-5]. The current indirect-drive ignition point design on the National Ignition Facility (NIF) [6] uses a 1.6 MJ laser pulse at peak power of 410 TW to accelerate the DT fuel to a peak implosion velocity of ~370 km/s [7]. The implosion must achieve a temperature of $T_i > 5$ keV in the central hot-spot and a high DT fuel compression with ρR_{fuel} ~1.5 g/cm^2 to achieve the predicted ignition neutron yield of ~20 MJ [7]. In recent high-compression experiments on NIF, a fuel areal density of ~1.3 g/cm^2 has been achieved with a fuel velocity of ~330 km/s [8,9]. While these two key performance parameters were close to the goal, the neutron yield was significantly reduced [8,9]. As the measured fuel compression was very close to the requirement, the main focus of the ignition program has shifted toward understanding and mitigating hydrodynamic instabilities and mix, reducing asymmetries, and increasing yield by entering the alpha-heating ("boot strapping") regime.

The layered deuterium-tritium (DT) implosions were modeled using 2D and 3D simulations intended to capture performance degradation due to instabilities and drive asymmetries [10]. These simulations over-predicted the yields by a factors of ~5 to ~30 for high-compression implosions. As a way to explain the measured performance, 2D simulations used large, un-physical multipliers (up to 3-5x) on the capsule surface roughness to bring simulated yields down to the measured levels [10]. This prompted the hypothesis that the instability growth factors were larger than in simulations. In addition, 2D and 3D simulations generally did not have a capability to fully include effects of ablator jets in the DT fuel, but the presence of mixed ablator material was correlated with

reduced experimental yields and temperatures in the high-compression layered DT implosions [11-13]. This suggested another hypothesis that ablator jet mix was also a major contributor to yield degradation.

Recent implosion experiments [14,15] using plastic (CH) capsules including deuterated (CD) layers filled high-purity tritium gas directly measured the ablator atomic mix using the DT reaction (D + T $\rightarrow$ ^{4}He + n) with the DT neutron yield and ion temperature. These experiments were modeled with 2D simulations including a turbulent K-L mix model that added the capability to include effects of the high-mode mix in simulations and to assess its importance to yield degradation [14]. To explain the experimental results, the simulations still required large surface roughness multipliers, consistent with modeling of high-compression layered DT implosions. The atomic-mix experiments suggested [14] that low-mode (with Legendre mode numbers $l < 100$) hydrodynamic instabilities were the primary cause of yield degradation, with atomic ablator-gas mix playing a secondary role.

There are several possible explanations for the need for such a large multiplier on the initial surface perturbation. The effective roughness could in fact be larger than assumed based on current metrology methods. The Rayleigh-Taylor [16,17] growth rates during the acceleration phase [1,2], or the pre-acceleration amplitudes established during the Richtmyer-Meshkov [18,19] instability phase could also be larger than simulated. Some seeds to the instability growth, including radiation asymmetry [20], dust grains and other localized defects, and the effect of the membrane ("tent") used to support the capsule [21,22] were not included in the simulations. The resultant elevated modulations could cause stronger performance degradation at peak compression, as suggested in

recent simulations [23,24]. Predictions of hydrodynamic instability growth need to be tested and validated by experiments to be used in the modeling of the previous implosion experiments and in the future designs. This Letter describes the first experiments to directly measure ablation-front hydrodynamic growth using x-ray radiography of pre-imposed, 2D sinusoidal perturbations at NIF. The measurements were focused on the fastest-growing modulations in the range of Legendre modes from 30 to 90. The goal was to test and validate hydrodynamic growth in simulations including the growth in the Richtmyer-Meshkov phase and the Rayleigh-Taylor phase at the outer ablation surface with moderate capsule convergence (2-3).

Figure 1(a) shows a picture of the target including a plastic capsule and a gold cone used in these experiments. The modulation growth was measured with through-foil x-ray radiography [25] using ~5.4-keV x-rays generated by the vanadium backlighter located 12 mm from the target center. The experiments were conducted with the drives and conditions similar to those used in high-compression layered DT implosions [8]. They were designed to test the hydrodynamic growth predictions used to model these DT layered implosions that achieved fuel areal densities of ~1.3 g/cm^2, peak fuel velocities of ~320-330 km/s, driven at peak radiation temperatures of ~300 eV [8]. The capsules had pre-imposed, 2D sinusoidal modulations at three wavelengths, 240 μm (corresponding to Legendre mode 30), 120 μm (mode 60), and 80 μm (mode 90). The gold cone constrained the backlighter x-rays to pass through a single wall of the shell, enabling high-quality radiographs of the growing modulations. The thickness of the gold cone was 150 μm, while the 800-μm inner diameter at the tip of the cone set the field of view for the radiography. The initial modulation amplitudes of 0.75 μm and 1.7 μm were used in

two shots with initial wavelengths of 240 μm and 120 μm, respectively. In another shot, side-by-side modulations at wavelength of 120 μm and 80 μm had initial amplitudes of 0.25 μm and 0.3 μm, respectively.

Figure 1(b) shows the lineout of the initial capsule perturbation amplitude vs azimuthal angle used in the shot with side-by-side mode 60 and 90 sinusoidal modulations. The pre-imposed modulations were high quality sinusoidal modulations with all higher harmonics kept below ~5% of the amplitude of the fundamental sinusoidal modulations. The variations of the modulation amplitudes were below ~10% over the whole area of interest for radiography. The nominal 209-μm thick plastic capsules with nominal 1120-μm outer diameters had the same Si-doped layers, as used in the previous DT layered implosion [8]. An extra 20-μm thick CH layer was used to replace the 69-μm thick DT layer to maintain the same shell mass as in the layered DT implosions. Current experiments followed a campaign that characterized the implosion shock timing and symmetry, as described in Ref. 26-30. Capsule and hohlraum details were also previously published (see Fig.1 of Ref. [31]). The experiments were driven with the shaped, 21-ns long laser pulse with peak power of ~350 TW and total laser energy of 1.3 MJ (shown in Fig. 2) using 184 beams of the NIF laser system. An additional eight overlapped beams were used to drive a 12.5-μm thick vanadium backlighter foil at peak laser intensity of ~5 $\times$ 10^{14} W/cm^2 with a pulse shape shown in Fig. 2. The experimental configuration was similar to previous backlighting experiments on NIF [26]. The differences included the additional gold cone, the material of backlighter (vanadium vs germanium), and the reduced thickness (80-μm vs 160-μm) of the high-density carbon (HDC) window placed

at the hohlraum wall. The 250-μm wide, and 900-μm long HDC windows provided a clear line of sight for the backlighter x-rays used for radiography.

Figure 3 shows examples of measured capsule x-ray radiographs captured on a framing camera for three different experiments with modes 30, 60, and side-by-side modes 60 and 90 using 20-μm wide slits. Four slit images were captured in each shot at four different times. The slit was oriented vertically, along the hohlraum axis, and also along the capsule 2D modulations. The 250-μm vertical size of the HDC window defined the integration extent of the slit images, while the field of view in the horizontal direction was defined by the 800-μm inner diameter of the Au cone. The slit was positioned 100 mm from the target center, while the detector, a framing camera [32], was located at 1300 mm from the target center, giving a magnification of ~12 for the imaging system. X-ray filters were used in these experiments both to protect the diagnostics from the debris generated by the hohlraum (using 150 μm polyimide filter) and to suppress x-ray emission above the vanadium K-edge to improve image contrast (using 12.5 μm thick vanadium filters). The temporal resolution of the images system was 100 ps, limited by the framing camera resolution [32]; while the spatial resolution was 20 μm in the horizontal direction, perpendicular to the slit. The x-ray background was measured using an additional shot and was subtracted from the radiography images during data analysis. This background consisted of the hard x-rays generated by hot electrons with energies >20 keV produced by laser-plasma interaction (LPI) processes in the hohlraum [33,34], and soft x-rays (~5-10 keV) backgrounds produced mainly between the capsule and the HDC window inside the hohlraum. The measured peak hard and soft x-ray backgrounds were ~10% and 2% of the backlighter signal. The spectral purity of the imaging system

was measured using a 30-μm thick aluminum strip placed in front of the framing camera on each shot. The measured strip attenuation was consistent with ~5.4-keV x-rays generated by the K-shell of the vanadium backlighter. The measured contrast was used in post-processing of the simulations to compare with experimental results, as discussed below. Optical-depth (OD) variations (used in the analysis below) were obtained by taking a natural logarithm of the framing-camera images after x-ray backgrounds were subtracted.

Figure 4 shows measured (symbols) and simulated (solid curves) modulation wavelengths as a function of time for experiments with mode 30 (initial wavelength of 240 μm), 60 (initial wavelength of 120 μm), and 90 (initial wavelength of 80 μm) modulations. The measurements were conducted for convergence ratios up to ~2, when the shell radius was decreased down to ~500 μm during the implosion. Simulations of these experiments were performed with two plastic equations of state (EOS) models [35], LEOS 5400 and LEOS 5370. Solid curves in Fig. 4 represent simulations with LEOS 5400, which were almost identical to the predictions with LOES 5370. The convergence ratio (defined as a ratio of the initial modulation wavelength to that at the time of the measurement) was used as a measure of the drive to compare with predictions. The good agreement between measured and simulated wavelength evolution validated the drive modeling used in the simulations [10].

Figure 5 shows the evolution of the measured and simulated amplitudes of the optical-depth modulations for the mode 30 with initial amplitude of 0.75 μm [Fig. 4(a)], the mode 60 with initial amplitudes of 1.7 and 0.25 μm [Fig. 4(b)], and the mode 90 with initial amplitude of 0.3 μm [Fig. 4(c)]. Simulations are shown by the solid and dashed

curves for two plastic equations of state (EOS) models [35], LEOS 5400 and LEOS 5370, respectively. Simulated optical-depth modulations were obtained by post-processing of simulations using 5.4-keV backlighter, and using measured spatial and temporal resolutions of the imaging system. The LEOS 5370 model predicted a slightly softer equation of state, compared to the LEOS 5400, but the difference was not significant in these measurements, as shown in Fig. 4. We note good agreement between data and simulations at all times, and in particular over a range of 50x in modulation growth for mode 60 (combining low and high initial amplitude data).

Figure 6 shows measured and calculated modulation optical-depth growth factors as a function of the modulation mode number at shell radius of 650 μm, corresponding to a measurement time of 20.3 ns. Simulations are shown by the solid and dashed curves for two plastic EOS models, LEOS 5400 and LEOS 5370, respectively. Effects of the spatial resolution were taken out in the measured experimental points for fair comparison. The good agreement between simulations and experiments indicated that instability growth was modeled well for the most unstable modulations in the high-convergence layered DT implosions in the acceleration phase at convergence ratios up to ~2. Therefore, future acceleration-phase instability experiments will be extended to shorter wavelengths and to higher convergence ratios up to ~5. In addition, deceleration phase instability experiments are also planned to test and validate simulation predictions near peak compression of the spherical implosions.

In conclusion, the first hydrodynamic instability growth measurements in indirectly-driven implosions measured instability growth of the pre-imposed modulations with Legendre mode numbers from 30 to 90 at the National Ignition Facility. The

capsules were imploded using ignition-relevant laser pulses, and ablation-front modulation growth was measured using x-ray radiography for a shell convergence ratio of ~2. The measured growth was in good agreement with that predicted, thus validating simulations for the fastest growing modulations with mode numbers up to 90 in the acceleration phase. Future experiments will be focused on measurements at higher convergence, higher-mode number modulations, and during the deceleration phase.

This work was performed under the auspices of the U.S. Department of Energy by Lawrence Livermore National Laboratory under Contract DE-AC52-07NA27344.

REFERENCES

[1] S. Atzeni and J. Meyer-ter-Vehn, *The Physics of Inertial Fusion: Beam Plasma Interaction, Hydrodynamics, Hot Dense Matter*, International Series of Monographs on Physics (Clarendon Press, Oxford, 2004).

[2] J. D. Lindl, *Inertial Confinement Fusion: The Quest for Ignition and Energy Gain Using Indirect Drive* (Springer-Verlag, New York, 1998).

[3] J. Nuckolls, L. Wood, A. Thiessen, and G. Zimmerman, Nature **239**, 139 (1972).

[4] J. Nuckolls, Physics Today **35**, 24 (1982).

[5] R. L. McCrory *et al.*, Nature **335,** 225 (1988).

[6] E. I. Moses, R. N. Boyd, B. A. Remington, C. J. Keane, and R. Al-Ayat, *Phys. Plasmas* **16**, 041006 (2009); G. H. Miller, E. I. Moses and C. R. Wuest, *Opt. Eng.* **43**, 2841 (2004).

[7] S. W. Haan, *et al*., Phys. Plasmas **18,** 051001 (2011).

[8] V. A. Smalyuk, *et al*., "Performance of high-convergence, layered DT implosions in power-scaling experiments at the National Ignition Facility", in press Phys.

Rev. Lett.

[9] M. J. Edwards, *et al.,* Phys. Plasmas **20**, 070501 (2013).

[10] D. S. Clark, *et al.,* Phys. Plasmas **20**, 056318 (2013).

[11] S. P. Regan, *et al.*, Phys. Plasmas **19**, 056307 (2012).

[12] S. P. Regan, *et al.*, Phys. Rev. Lett. **111**, 045001 (2013).

[13] T. Ma, *et al*., Phys. Rev. Lett. **111**, 085004 (2013).

[14] V. A. Smalyuk, *et al*., "Measurements of ablator-gas mix in indirectly-driven implosions at the National Ignition Facility", submitted Phys. Rev. Lett.

[15] D. B. Sayre, *et al*., Phys. Rev. Lett. **111**, 052501 (2013).

[16] Lord Rayleigh, Scientific Papers II (Cambridge, England, 1900).

[17] G.I. Taylor, Proc. R. Soc. London, Ser. A **201**, 192 (1950).

[18] R. D. Richtmyer, Commun. Pure Appl. Math. **13**, 297 (1960).

[19] E. E. Meshkov, Izv. Acad. Sci. USSR Fluid Dynamics **4**, 101 (1969).

[20] R. H. H. Scott, *et al*., Phys. Rev. Lett. **110**, 075001 (2013).

[21] O.L. Landen, *et. al*., Plasma Phys. Control. Fusion **54,** 124026 (2012).

[22] S. W. Haan, *et al*,. Fus. Sci. and Tech. 63, 67 (2013).

[23] S. V. Weber, *et al*., "NIF symmetry capsule modeling", Bull. Am. Phys. Soc. **58**, 195 (2013).

[24] D. S. Clark, *et al*., "Progress in modeling ignition experiments on the National

Ignition Facility", to be published in the Proceedings of the Eighth International Conference on Fusion Sciences and Applications, Nara, Japan (2013).

[25] V. A. Smalyuk, *et al.,* Phys. Rev. Lett. **103**, 105001 (2009).

[26] D. G. Hicks, *et al*., Phys. Plasmas **19**, 122702 (2012).

[27] D. A. Callahan, *et al*., Phys. Plasmas **19**, 056305 (2012).

[28] N. B. Meezan, *et al.,* Phys. Plasmas **20**, 056311 (2013).

[29] H. F. Robey, *et al.*, Phys. Rev. Lett. **108**, 215004 (2012).

[30] H. F. Robey, *et al.*, Phys. Plasmas **19**, 042706 (2012).

[31] S. H. Glenzer, *et al.*, Phys. Plasmas **19**, 056318 (2012).

[32] S. Glenn, *et al.*, Rev. Sc. Instrum. **83**, 10E539 (2010).

[33] W. L. Kruer, The Physics of Laser Plasma Interactions (Addison-Wesley) 1988.

[34] T. Döppner, *et al.,* Phys. Rev. Lett. **108**, 135006 (2012).

[35] S. Hamel, *et al.,* Phys. Rev. B **86** 094113 (2012).

FIGURE CAPTIONS

FIG. 1. (a) A picture of the capsule including pre-imposed 2D modulations and gold cone oriented along a diagnostic line of site. The outer circular feature is the equatorial diagnostic band before hohlraum assembly. (b) The initial amplitude vs the azimuthal angle for side-by-side, 2D sinusoidal modulations with mode numbers of 60 and 90, as measured for one of the capsules used in the experiments.

FIG. 2. Laser pulse shape used in the experiments for hohlraum drive had a peak power of ~350 TW and total energy of ~1.3 MJ, while a backlighter pulse shape had a peak power of ~4 TW.

FIG. 3. Examples of measured radiographs are shown for three experiments with modulations at mode numbers of 30, 60, and side-by-side modes 60 and 90.

FIG. 4. Measured and simulated (solid curves) modulation wavelengths as a function of time for experiments with mode 30 (with initial wavelength of 240 μm), 60 (with initial wavelength of 120 μm), and 90 (with initial wavelength of 80 μm) modulations. The good agreement between measured and simulated wavelength evolution validates the drive modeling used in the simulations.

FIG. 5. Evolution of the measured and simulated amplitudes of the optical-depth modulations for (a) mode 30 with initial wavelength of 240 μm and amplitude of 0.75 μm, (b) mode 60 with initial wavelength of 120 μm and amplitudes of 1.7 and 0.25 μm,

and (c) mode 90 with initial wavelength of 80 μm and amplitude of 0.3 μm. Simulations are shown by the solid and dashed curves for two plastic equations of state (EOS) models, LEOS 5400 and LEOS 5370, respectively.

FIG. 6. Measured and calculated linear growth factors for optical-depth modulations as a function of the modulation mode number are shown at shell radius of 650 μm, corresponding to a measurement time of 20.3 ns. Simulations are shown by the solid and dashed curves for two plastic EOS models, LEOS 5400 and LEOS 5370, respectively.

Figure 1

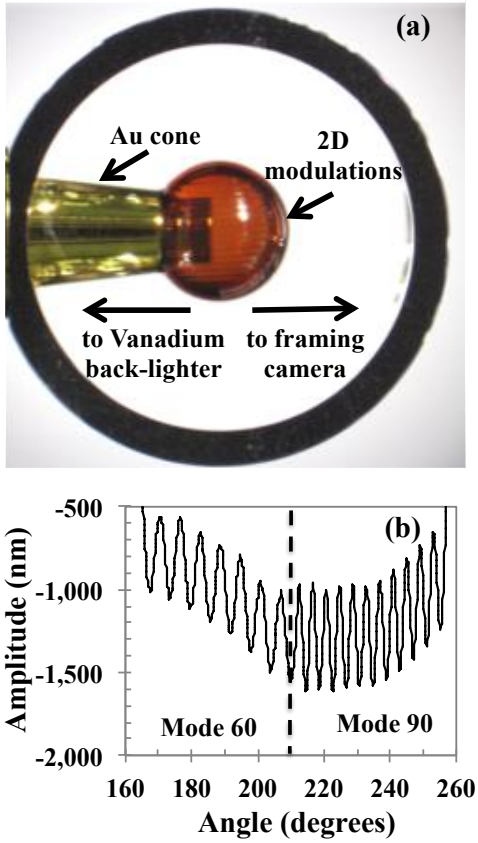
(a)
Au cone
2D
modulations
to Vanadium
back-lighter
to framing
camera
(b)
-500
-1,000
-1,500
-2,000
Amplitude (nm)
Mode 60
Mode 90
160
180
200
220
240
260
Angle (degrees)

Figure 2

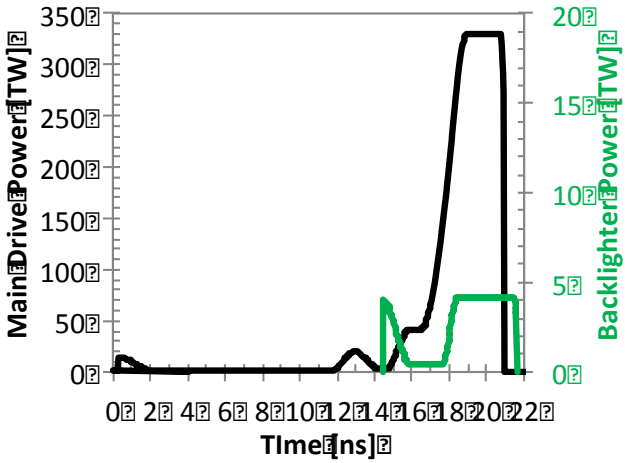
Main Driver Power [TW]
Backlighter Power [TW]
Time [ns]
350
300
250
200
150
100
50
0
20
15
10
5
0
0 2 4 6 8 10 12 14 16 18 20 22

Figure 3

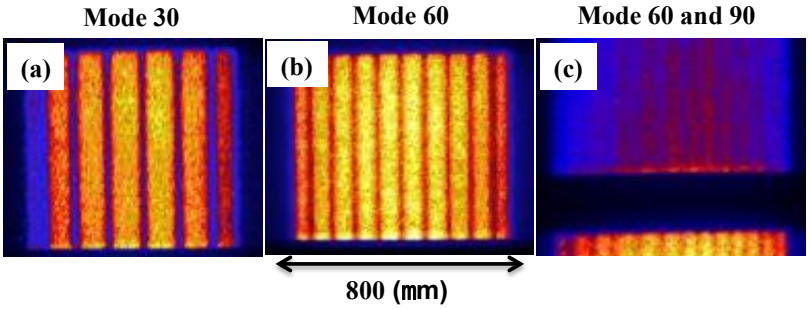

Figure 4

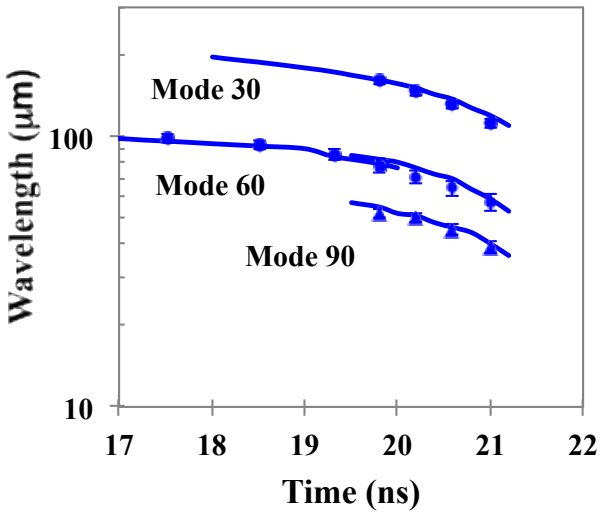
Mode 30
Mode 60
Mode 90
Wavelength (μm)
100
10
17
18
19
20
21
22
Time (ns)

Figure 5

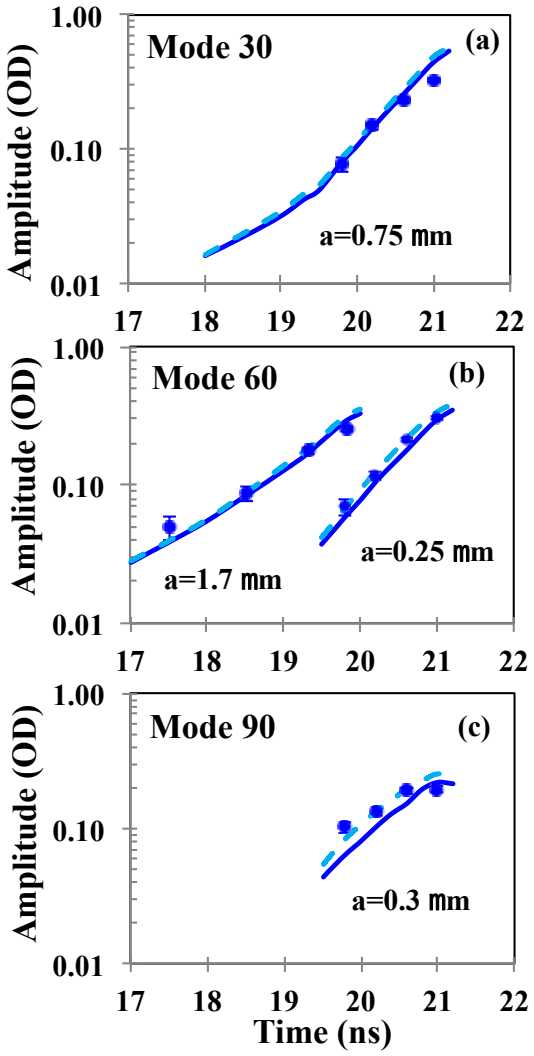
Mode 30
(a)
a=0.75 mm
Mode 60
(b)
a=1.7 mm
a=0.25 mm
Mode 90
(c)
a=0.3 mm
Amplitude (OD)
1.00
0.10
0.01
17
18
19
20
21
22
Time (ns)

Figure 6

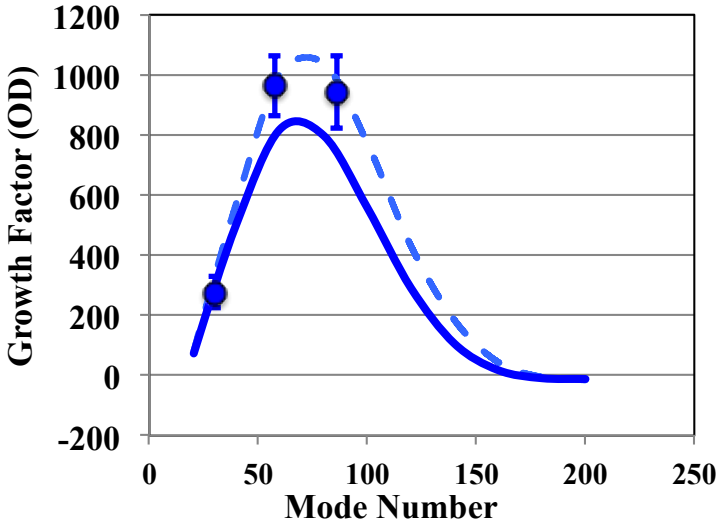
1200
1000
800
600
400
200
0
-200
Growth Factor (OD)
0
50
100
150
200
250
Mode Number